

Accurate effective harmonic potential treatment of the high-temperature cubic phase of Hafnia

Sebastian Bichelmaier,^{1,2} Jesús Carrete,¹ Michael Nelhiebel,² and Georg K. H. Madsen^{1,*}

¹*Institute of Materials Chemistry, TU Wien, A-1060 Vienna, Austria*

²*KAI GmbH, Europastrasse 8, A-9524 Villach, Austria*

(Dated: October 12, 2021)

HfO₂ is an important high- κ dielectric and ferroelectric, exhibiting a complex potential energy landscape with several phases close in energy. It is, however, a strongly anharmonic solid, and thus describing its temperature-dependent behavior is methodologically challenging. We propose an approach based on self-consistent, effective harmonic potentials and higher-order corrections to study the potential energy surface of anharmonic materials. The introduction of a reweighting procedure enables the usage of unregularized regression methods and efficiently harnesses the information contained in every data point obtained from density functional theory. This renders the approach highly efficient and a promising candidate for large-scale studies of materials and phase transitions. We detail the approach and test it on the example of the high-temperature cubic phase of HfO₂. Our results for the thermal expansion coefficient, $\alpha_V \approx 3.3 \times 10^{-5} \text{ K}^{-1}$, are in agreement with existing experimental ($\approx 4(1) \times 10^{-5} \text{ K}^{-1}$) and theoretical ($\approx 5(1) \times 10^{-5} \text{ K}^{-1}$) work. Likewise, the bulk modulus agrees well with experiment. We show the detailed temperature dependence of these quantities.

Keywords: cubic hafnia, effective harmonic potentials, high-temperature density functional theory

I. INTRODUCTION

One of the biggest drawbacks of density functional theory (DFT) calculations is the lack of temperature-induced effects. However, due to the exponential growth in computing power and continuous methodological developments, the previously prohibitively expensive calculations necessary to remedy that shortcoming are becoming viable for the investigation of new materials. Consequently, the inclusion of temperature is a prominent theme in many current computational efforts¹⁻⁸.

In the present study we focus on hafnia, HfO₂, which has a multi-faceted phase diagram⁹ and numerous industrially relevant applications, ranging from a high- κ gate dielectric for semiconductors in its amorphous¹⁰ and (more recently suggested) tetragonal phase¹¹, to a ferroelectric in its orthorhombic states¹² for e. g. non-volatile memory applications¹³.

An accurate DFT treatment of its temperature-dependent behavior has proven difficult to achieve in previous theoretical efforts¹⁴. In the simplest approach, the effect of temperature is included by means of the harmonic approximation (HA), where the phonon modes of the system are described as independent harmonic oscillators. The second-order interatomic force constants (IFCs) are obtained by applying small displacements and mapping the corresponding forces induced by them. However, in the case of structures governed by anharmonic potential energy surfaces (PES), the HA might yield imaginary frequencies, thus indicating mechanical instability, even when experiments confirm the existence of those structures.

Ab-initio molecular dynamics (AIMD) approaches¹⁵

can, in principle, treat such temperature-stabilized structures, but obtaining the free energy of reasonably complex systems through thermodynamic integration proves to be a resource-intensive task and quickly becomes intractable. Moreover, AIMD treats the nuclear motion in a completely classical fashion, and therefore cannot capture effects such as zero-point motion, which can be relevant for e.g. accurately describing the vibrations of light and strongly bonded atoms.

An emerging category of alternatives to AIMD can be labelled as effective harmonic potentials (EHP). The idea goes back to 1955¹⁶ and in essence involves determining the best HA to the part of the PES which dominates nuclear motion. Temperature dependent contributions to the free energy are then included using independent harmonic oscillators based on these EHPs. EHPs have proven to be a rich starting point for understanding temperature dependent behavior using ab-initio methods and, as computational power has become available, prompted various implementations and formulations of the underlying theory^{3,6,7,17-20}. The implementations mainly differ in how the PES is sampled with methods including stochastic sampling and molecular dynamics trajectories as well as how the deviation between the EHP and the PES is accounted for.

In the present study we focus on the high-temperature cubic (Fm $\bar{3}$ m) hafnia phase (c-HfO₂). c-HfO₂ is an example of a temperature stabilized structure where the small displacement HA yields imaginary frequencies¹⁴. We show how the use of reweighting in combination with unregularized regression can be employed to obtain the temperature-dependent EHP. Furthermore, the correction for the deviation between the

EHP and the true DFT PES is discussed in detail. We compare our results to the available AIMD calculations and experiments.

II. METHOD

A. Background

A system described by a Hamiltonian $\hat{\mathcal{H}}$ is in a state of thermal equilibrium at constant volume, temperature and number of particles when its free energy

$$\mathcal{F}[\hat{\rho}] = \text{tr}(\hat{\rho}\hat{\mathcal{H}}) + T\text{tr}(\hat{\rho}\log\hat{\rho}) \quad (1)$$

is at a minimum. This equilibrium state is described by a particular quantum mechanical density matrix, $\hat{\rho}$, which, were it known, would provide access to the whole thermodynamics of the system. However, it is impossible for all but trivial model systems to solve this problem exactly.

The EHP can be formulated as a variational problem^{20,21} where a trial density matrix, $\hat{\rho}$, which exactly solves a corresponding trial Hamiltonian, \hat{H} , is introduced. \hat{H} differs from the true Hamiltonian $\hat{\mathcal{H}}$ only by the form of the potential energy operator \hat{V} , as opposed to \hat{V} . Minimizing the free energy with respect to the trial density matrix is guaranteed by the Gibbs-Bogoliubov inequality²² to provide an upper bound on the free energy

$$\mathcal{F}[\hat{\rho}] \leq F[\hat{\rho}] = \mathcal{F}[\hat{\rho}] + \text{tr}[\hat{\rho}(\hat{V} - \hat{V})] = \mathcal{F}[\hat{\rho}] + F_{\text{corr}}, \quad (2)$$

In the harmonic approximation, the trial potential is parametrized as

$$\langle \vec{u} | \hat{V} | \vec{u} \rangle = V(\vec{u}) = \sum_{ij} \frac{1}{2} u_i \Phi_{ij} u_j, \quad (3)$$

in terms of the displacements from the minimum-energy configuration, \vec{u} , and the second-order force constants, Φ_{ij} , whose eigenvalues and eigenvectors

$$\Phi_{ij} = \sum_{\lambda} \omega_{\lambda}^2 \epsilon_{\lambda i} \epsilon_{\lambda j}^*, \quad (4)$$

will hereafter be denoted by ω_{λ}^2 and $\vec{\epsilon}_{\lambda}$. The indices i, j denote the ions and the Cartesian directions. Within the harmonic approximation, the projection onto real space of the trial density matrix can be expressed in closed form

$$\langle \vec{u} | \hat{\rho} | \vec{u} \rangle = \tilde{\rho}(\vec{u}) = \frac{1}{\sqrt{(2\pi)^{3N}} \sqrt{|C|}} e^{-\frac{1}{2} \vec{u} C^{-1} \vec{u}}. \quad (5)$$

The covariance matrix C can be obtained from the aforementioned ω_{λ} and $\vec{\epsilon}_{\lambda}$ through a well-known result of quantum statistical mechanics

$$C_{ij} = \frac{\hbar}{2\sqrt{M_i M_j}} \sum_{\lambda} \frac{1}{\omega_{\lambda} \tanh \frac{\hbar\omega_{\lambda}}{2k_B T}} \epsilon_{\lambda i} \epsilon_{\lambda j}^*, \quad (6)$$

where M correspond to the masses of the ions. Furthermore, the expression for the free energy, $\mathcal{F}[\hat{\rho}]$, is given by

$$\mathcal{F}(T) = \sum_{\lambda} \hbar\omega_{\lambda} \left(\frac{1}{2} + k_B T \log \left[1 - \exp \left\{ -\frac{\hbar\omega_{\lambda}}{k_B T} \right\} \right] \right). \quad (7)$$

\mathcal{F} depends directly on the temperature T and indirectly on the harmonic trial potential through ω_{λ} , Eq. (4). The optimal trial potential thus depends on the temperature. Ignoring F_{corr} , Eq. (2), and the temperature-dependence of the effective potential results in the well-known quasi-harmonic approximation.

B. Temperature-dependent effective potentials

We implement the search for the optimal EHP by approximating the real-space density matrix by means of canonical importance sampling and treating the interdependence of \mathcal{F} and Φ as a self-consistent problem. When self consistency is reached, this corresponds to minimizing $F[\hat{\rho}]$.

The starting point is the second-order force-constant matrix, and corresponding potential $V^{(1)}$, obtained through small displacements as implemented in Phonopy²³. From the eigenvalues and eigenvectors and the temperature of interest the associated trial density, $\tilde{\rho}^{(1)}$, is obtained through Eqs. (5) and (6). We replace the imaginary square roots of possible negative eigenvalues from intermediate steps with their modulus. From this probability density the first set of displacements, $\mathcal{S}^{(1)}$, are drawn. A new EHP is obtained by calculating the potential energies and forces corresponding to the displacements using DFT and finding the parametrization of the force constants in Eq. (4) which best represent the relationship between forces and displacements, as will be discussed below. The iterative process then progresses by constructing a new density matrix using Eqs. (5) and (6). To aid convergence, the new trial density matrix, $\tilde{\rho}^{(k)}$, is obtained through a Pulay mixing scheme²⁴ with a memory of $n = 5$ and a mixing parameter of $\alpha = 0.1$, as commonly used. A new set of displacements is now drawn and the process continues until convergence is reached.

To efficiently use all the data obtained from DFT, the

reweighting factor¹⁷ is introduced

$$w_m^{(g \rightarrow k)} = \frac{\tilde{\rho}^{(k)}(\vec{u}_m^{(g)})}{\tilde{\rho}^{(g)}(\vec{u}_m^{(g)})}, \quad (8)$$

Thereby displacement vectors, $\vec{u}_m^{(g)}$, belonging to a set drawn in a previous iteration, $\mathcal{S}^{(g)}$, and their corresponding forces and potential energies can be included as if they belong to the current set, $\mathcal{S}^{(k)}$.

Using the reweighting factors significantly increases the amount of available data and allows using an unregularized fitting procedure to obtain the force constant matrix. The trial potential for iteration k is found by finding the force constants which minimize the weighted sum of the least-squares deviations from the calculated forces, i. e. ,

$$\sum_g \sum_m w_m^{(g \rightarrow k)} \left\| \vec{f}_m^{(g)} + \Phi \vec{u}_m^{(g)} \right\|_2^2 \quad (9)$$

In Fig. 1 the free energy evaluated according to Eq. (7) is shown as a function of the iterations until convergence for the 0K equilibrium volume using a temperature of $T = 2500$ K. Typically the convergence criterion of $\Delta\mathcal{F} < 2.5$ meV f.u.⁻¹ is reached in 10 – 15 iterations when 5 structures are added per iteration for the initial temperature point, totaling 50 - 75 DFT runs.

Alternatively, a penalty

$$\left(\sum_g \sum_m w_m^{(g \rightarrow k)} \left\| \vec{f}_m^{(g)} + \Phi \vec{u}_m^{(g)} \right\|_2^2 + \alpha \|\Phi\|_1 \right) \quad (10)$$

can be defined. This is known as the LASSO minimization target function. The α parameter determines the strength of the L_1 regularization and promotes sparsity of the force constant matrix, which can be a computational advantage²⁵. By partitioning the data into five complementary subsets and minimizing Eq. (10) for a range of α -values, the regularization strength can be tuned to provide the model which generalizes best, i.e. has the best performance on the subsets not used for obtaining the force constants. This so-called 5-fold cross validation procedure²⁶ is performed at every step of the iteration. In Fig. 1 we compare the convergence behaviour at $T = 2500$ K for the 0K equilibrium structure. Notably, the α parameter quickly approaches zero as the calculation progresses. This is understandable as regularization is typically applied when fitting samples which insufficiently cover the sample space. Thus, as the amount of data points available for fitting increases, every fold in the cross validation procedure will be more and more equally representative of the rest, so the L_1 penalty will actually hinder minimizing Eq. (10) and will be forced towards zero by the algorithm itself, effectively resulting in Eq. (9).

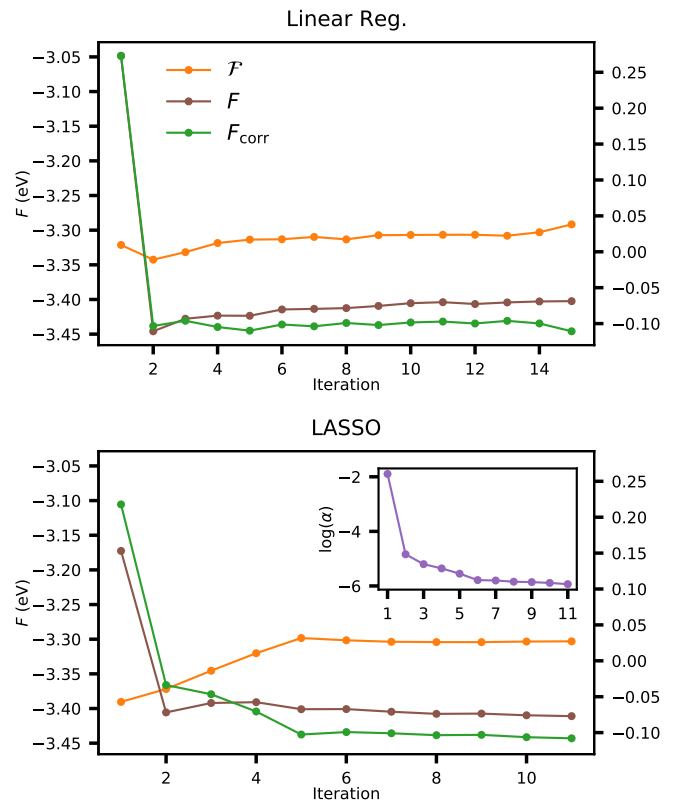


Figure 1. Convergence of the free energy contributions with iterations for the exemplary case of the 0K equilibrium structure, $V_0 = 32.62 \text{ \AA}^3$, at $T = 2500$ K. The upper plot is for a least squares penalty function and the lower for LASSO. The total free energy, F , and the harmonic contribution, \mathcal{F} , are given w.r.t. the y-axis to the left and F_{corr} with respect to the y-axis to the right. In every iteration 5 new structures are added.

We have chosen the unregularized least-squares approach, Eq. (9) for two reasons: We are, for all but the first few iterations, confronted with an overdetermined system, as only a total of 52 independent force constants remain after considering symmetry and the cut-off and every sample provides 576 force-displacement pairs. Furthermore, if a non-zero L_1 -penalty was indeed used throughout the calculation, the force constants obtained would not fulfill the property of minimizing the free energy once self-consistency is reached⁷. As argued above, the regularization parameter must approach zero, because the coverage increases with every iteration. While we would presumably not have arrived at an artificially increased free energy, using LASSO only provided a minor speed up, while introducing additional uncertainty in the results.

The correction term, F_{corr} , has previously been calculated by representing the DFT PES by a simpler

form^{17,20} or by using the trajectory obtained from AIMD^{6,27}. We calculate F_{corr} directly from the DFT potential energies obtained from the same sampling as used for determining the trial EHP, Eq. (9), as a weighted average

$$F_{\text{corr}} = \frac{1}{W} \sum_g \sum_m w_m^{(g \rightarrow k)} (\mathcal{V}(\vec{u}_m^{(g)}) - V^{(k)}(\vec{u}_m^{(g)})), \quad (11)$$

where W is the sum of all the weights. Similar to the EHP the reweighting allows all DFT calculations to be used for obtaining F_{corr} and Fig. 1 illustrates that the convergence is also comparable, meaning that convergence of the total free energy, F , is reached within 10 – 15 iterations.

It is straightforward to extend the formalism described above to reuse samples drawn at temperature T_1 for a different temperature T_2 , by building reweighting factors accounting for this. This provides a fast way to calculate force constants at temperatures near T_1 . At temperatures more different from T_1 the sample set might not be adequate anymore, necessitating augmentation by additional DFT runs. As an example we mention that using the displacements and forces obtained for $T_1 = 2500$ K, Fig. 1, at $T_2 = 2100$ K, but reweighted according to Eq. (8) results in convergence after adding only two additional iterations. Once convergence has been obtained for a mesh of temperatures, free energies can be obtained at intermediate temperatures without additional DFT calculations. As a measure for when additional calculations are necessary, we use the effective number of samples,

$$w_{\text{eff}}^{(k)} = \frac{\left(\sum_g \sum_m w_m^{(g \rightarrow k)} \right)^2}{\sum_g \sum_m (w_m^{(g \rightarrow k)})^2}. \quad (12)$$

As can be observed in in Fig. 2, the number of effective samples is indeed an excellent metric for the trustworthiness of the data at a given temperature. However, it would be grossly inefficient to augment the data if the poorly-sampled regions are small and constrained and the surrounding points are described by the existing samples well-enough. To prevent this, we apply a smoothing spline weighted with the effective samples to $F(T)$. This procedure avoids artifactual oscillations in later results.

C. Computational details

The DFT calculations were performed using the Vienna Ab Initio Simulation Package (VASP)^{28–30}, where we utilized the Perdew-Berke-Ernzerhof (PBE) exchange and correlation potential³¹ along with an energy cutoff of 600 eV. The force calculations for the

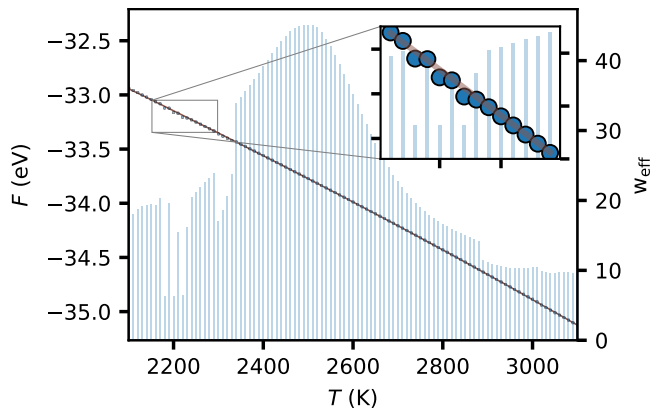


Figure 2. Free energy and effective samples as a function of temperature at +2% deformation, i.e. a volume of 34.62 \AA^3 . In regions where the effective samples, as shown by the bars in the background, are low, the free energy shows discontinuous behaviour. The brown line is a smoothing spline using the effective samples as weights, whereas the blue points are the data points.

phonons were performed in a $4 \times 4 \times 4$ supercell using just the Γ -point. We used Phonopy²³ with the non-analytical correction described in³² for obtaining the initial small displacements force constants. The descriptors for fitting the force constants [Eq. (9) and Eq. (10)] are obtained using scikit-learn²⁶ and the cluster formalism established in Ref. 33 given a pre-defined cutoff $r_{\text{cut}} = 7 \text{ \AA}$.

We performed the steps outlined above for various deformations of the 0 K equilibrium structure; we included volumes from $V = 30.70 \text{ \AA}^3/\text{f.u.}$ to $37.77 \text{ \AA}^3/\text{f.u.}$, as well as various temperatures ranging from 2100 K to 3100 K. To arrive at a simple but general analytical expression we then fit the free energies using,

$$F(V; T) = c_0 + \frac{c_1}{V^{1/3}} + \frac{c_2}{V^{2/3}} + \frac{c_3}{V}, \quad (13)$$

achieving an average deviation between actual and fitted free energy of less than 7 meV f.u.^{-1} , which corresponds to less than 3 meV atom^{-1} . This allows for finding the equilibrium lattice parameter and volume at every temperature point of interest with a high accuracy.

III. RESULTS

We settled on a temperature range from 2100 K to 3100 K to ensure full coverage of the stable region of c-HfO₂, 2800 K to 3100 K³⁴, with the upper bound close to the melting temperature. To accurately treat

this temperature range, we performed an initial self-consistent run at $T_1 = 2500$ K, augmented it with samples at $T_2 = 2100$ K and, guided by the effective sample size, Eq. (12), included $T_3 = 3000$ K for some deformations.

As an example, we show the phonon band structure of the 0 K equilibrium structure in Fig. 3, as obtained using small displacements and using the EHP at elevated temperatures. As can be seen c-HfO₂ shows an instability in the small displacements (0 K) phonon spectrum at $X = (0, 1/2, 1/2)$ in the Brillouin zone, which, in the structurally very similar ZrO₂ has been linked to the cubic-to-tetragonal phase transition³⁵. Within the studied temperature range, we see a continuous hardening (shown in the inset) of said mode indicating that temperature-induced anharmonic effects are stabilizing this phase. For the additional volumes that were studied (-6% to 16% volume changes) we find a similar behaviour and can report stable phonon spectra for the whole volume and temperature range.

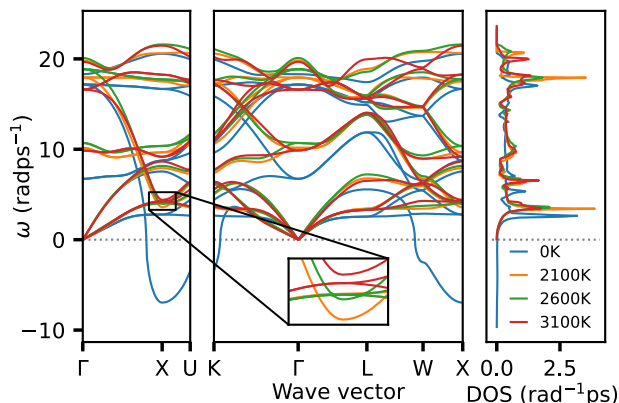


Figure 3. Phonon band structure and density of states of c-HfO₂ at the 0 K equilibrium volume. The soft mode at 0 K indicated by the negative frequencies at X in blue continuously hardens as temperature increases and the structure becomes stable.

The absence of imaginary phonon frequencies make it possible to calculate the vibrational contribution to the free energy according to Eq. (7). Fig. 4 depicts the volume dependence of the free energy at four different temperatures. Eq. (13), captures the behavior of c-HfO₂ across the studied temperature range and as expected the equilibrium volume increases with temperature. Interestingly, F_{corr} not only shifts the curve to lower energies, $\mathcal{O}(100 \text{ meV f.u.}^{-1})$, but it also changes the positions of the minima. As expected, F_{corr} gets larger with temperature, i. e. with increasing anharmonic contributions to the relevant parts of the PES. As a result, the contribution generally favors larger volumes and can be expected to be important for a correct predicting of thermal expansion.

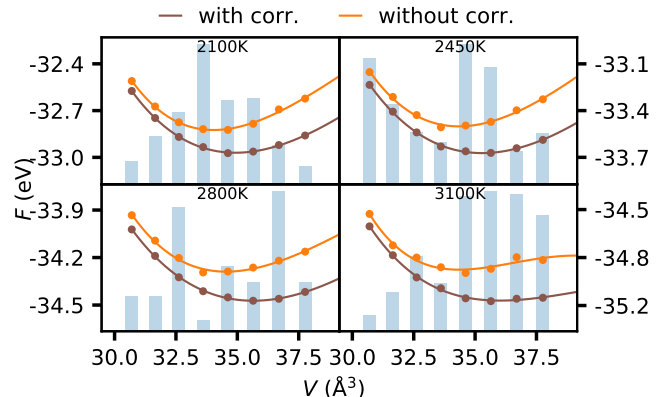


Figure 4. Comparison of the free energies obtained for various volumes and temperatures with and without the correction. The solid lines are the fitted SJEOS as described in Eq. (13), while the bars in the background are representing the effective sample size from Eq. (12). The correction shifts the free energy downwards and towards larger volumes.

The role of the correction term becomes even more apparent when looking at the thermal expansion in Fig. 5. Comparing the unit-cell volume of c-HfO₂ with experimental and theoretical results from literature,^{9,36} illustrates how neglecting F_{corr} will provide underestimated unit cell volume in situations where anharmonicities contribute a significant portion of the total energy. Such situations can arise when describing materials that are inherently anharmonic, or generally for materials at elevated temperatures. HfO₂ is in our study subject to both of these circumstances and thus any description not taking the anharmonic correction into account is bound to lead to inaccurate conclusions. Even when F_{corr} is included, a constant offset of about 0.5 \AA^3 , or 1.2% , can be observed. This can be attributed to inherent approximations of the chosen DFT functional. It is not possible to prove this as no 0 K experimental data exists to compare with. However, it is worth noting that the AIMD study reported in Ref. 36 (employing the same PBE functional), also finds slightly lower volumes than experiment.

The calculated thermal expansion coefficient [see inset in Fig. 5] is approximately constant, $3.3 \times 10^{-5} \text{ K}^{-1}$, until an increase in thermal expansion can be seen as the melting temperature, $T_m \approx 3100$ K, is approached. The thermal expansion coefficient is not impacted by a small constant offset, and our results are within or very close to the uncertainty, indicated by a red bar, of the experimental average over the range from 2800 K to 3100 K, $4(1) \times 10^{-5} \text{ K}^{-1}$, obtained by Hong. et al.³⁶. The volume data from Tobase et. al⁹ would result in $\alpha_V = 4.39 \times 10^{-5} \text{ K}^{-1}$, over the region of approximately 2823 K to 3043 K. However, due to the large uncertainty in the volume measurements, the error bar

would span about $8.3 \times 10^{-5} \text{ K}^{-1}$, and hence it is not shown in the graph.

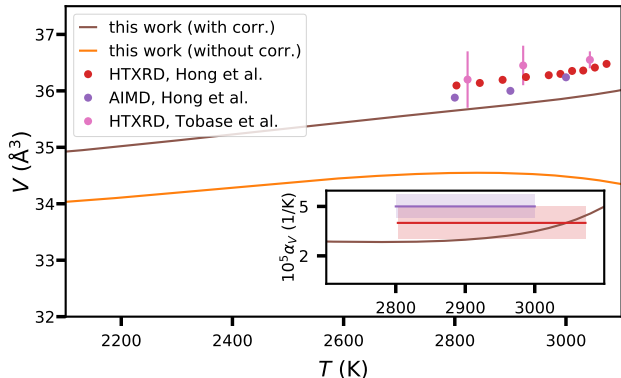


Figure 5. The unit-cell volume expansion as a function of temperature obtained in this work with (without) correction in brown (orange). The results are compared to experimental data^{9,36} and ab-initio molecular dynamics calculations³⁶. The thermal expansion coefficient, $\alpha_V = \frac{1}{V} \left(\frac{\partial V}{\partial T} \right)_p$, is shown in the inset. The shaded area in the inset indicates the experimental uncertainty.

Finally, we report the temperature dependence of the c-HfO₂ bulk modulus. Due to the fact that the second derivative of Eq. (13) w.r.t. lattice parameter (or volume) is not linear, the bulk modulus obtained by our method is naturally dependent on the volume at a given pressure at which it is evaluated. Evaluated at 0 GPa we find a bulk modulus of $B_0 = 180$ GPa, which decreases to 120 GPa over the range of 2100 K to 3100 K. This drastic softening is expected as we are approaching the melting point of the material. In their recent study, Irshad et al.³⁷, have measured the bulk modulus of pressure-stabilized, nanocrystalline c-HfO₂ at ambient temperature, finding $B_0 = 242(16)$ GPa. Apply-

ing a small pressure of 4 GPa (corresponding to a volume change of 1.5%) to our result, yields a comparable bulk modulus of about 210 GPa at 2100 K, decreasing to 170 GPa at 3100 K.

IV. CONCLUSION

The behavior of c-HfO₂ in the high-temperature regime was studied using effective harmonic potentials. At elevated temperatures the unstable mode exhibited by the cubic structure hardens, resulting in a stable phonon spectrum. It was shown that, without consideration of the anharmonic correction term, an accurate description of this phase is not possible and it is conjectured that this term is crucial throughout a broad spectrum of high-temperature materials studies.

The thermal expansion behavior reported, $\alpha_V = 3.3 \times 10^{-5} \text{ K}^{-1}$, is in good agreement with the existing experimental and theoretical data, if averaged over the same temperature range. In the range of 2100 K to 3100 K the bulk modulus of c-HfO₂ exhibits a drastic elastic softening from 180 GPa to 120 GPa, which can be expected as the melting point of the compound is estimated to be around 3100 K.

Ultimately, taking into consideration the difficulties of precise measurements at these high temperatures, as well as the computational cost of the alternatives, effective harmonic potentials can provide valuable insights at manageable cost when studying high-temperature phases.

ACKNOWLEDGEMENTS

AI4DI receives funding within the Electronic Components and Systems for European Leadership Joint Undertaking (ESCEL JU) in collaboration with the European Union's Horizon2020 Framework Programme and National Authorities, under grant agreement n° 826060.

* Correspondence email address: georg.madsen@tuwien.ac.at

¹ J. Xie, S. de Gironcoli, S. Baroni, and M. Scheffler, Phys. Rev. B **59**, 970 (1999).

² B. Grabowski, T. Hickel, and J. Neugebauer, Phys. Rev. B **76**, 024309 (2007).

³ P. Souvatzis, O. Eriksson, M. I. Katsnelson, and S. P. Rudin, Phys. Rev. Lett. **100**, 095901 (2008).

⁴ B. Grabowski, L. Ismer, T. Hickel, and J. Neugebauer, Phys. Rev. B **79**, 134106 (2009).

⁵ O. Hellman, I. A. Abrikosov, and S. I. Simak, Phys. Rev. B **84**, 180301 (2011).

⁶ O. Hellman, P. Steneteg, I. A. Abrikosov, and S. I. Simak, Phys. Rev. B **87**, 104111 (2013).

⁷ A. van Roekeghem, J. Carrete, and N. Mingo, Computer Physics Communications **263**, 107945 (2021).

⁸ S. Ehsan, M. Arrigoni, G. K. H. Madsen, P. Blaha, and A. Tröster, Phys. Rev. B **103**, 094108 (2021).

⁹ T. Tobase, A. Yoshiasa, H. Arima, K. Sugiyama, O. Ohtaka, T. Nakatani, K.-i. Funakoshi, and S. Kohara, physica status solidi (b) **255**, 1800090 (2018).

¹⁰ G. D. Wilk, R. M. Wallace, and J. M. Anthony, Journal of Applied Physics **89**, 5243 (2001).

¹¹ D. Fischer and A. Kersch, Journal of Applied Physics **104**, 084104 (2008).

- ¹² T. S. Böske, J. Müller, D. Bräuhaus, U. Schröder, and U. Böttger, *Applied Physics Letters* **99**, 102903 (2011).
- ¹³ J. Müller, P. Polakowski, S. Mueller, and T. Mikolajick, *ECS Journal of Solid State Science and Technology* **4**, N30 (2015).
- ¹⁴ T. D. Huan, V. Sharma, G. A. Rossetti, and R. Ramprasad, *Phys. Rev. B* **90**, 064111 (2014).
- ¹⁵ R. Iftimie, P. Minary, and M. E. Tuckerman, *Proceedings of the National Academy of Sciences* **102**, 6654 (2005).
- ¹⁶ D. Hooton, *The London, Edinburgh, and Dublin Philosophical Magazine and Journal of Science* **46**, 422 (1955).
- ¹⁷ I. Errea, M. Calandra, and F. Mauri, *Phys. Rev. Lett.* **111**, 177002 (2013).
- ¹⁸ T. Tadano and S. Tsuneyuki, *Phys. Rev. B* **92**, 054301 (2015).
- ¹⁹ R. Stern and G. K. H. Madsen, *Phys. Rev. B* **94**, 144304 (2016).
- ²⁰ L. Monacelli, R. Bianco, M. Cherubini, M. Calandra, I. Errea, and F. Mauri, *Journal of Physics: Condensed Matter* **33**, 363001 (2021).
- ²¹ I. Errea, M. Calandra, and F. Mauri, *Phys. Rev. B* **89**, 064302 (2014).
- ²² A. Isihara, *Journal of Physics A: General Physics* **1**, 539 (1968).
- ²³ A. Togo and I. Tanaka, *Scripta Materialia* **108**, 1 (2015).
- ²⁴ P. Pulay, *Journal of Computational Chemistry* **3**, 556 (1982).
- ²⁵ E. Fransson, F. Eriksson, and P. Erhart, *npj Computational Materials* **6**, 135 (2020).
- ²⁶ F. Pedregosa, G. Varoquaux, A. Gramfort, V. Michel, B. Thirion, O. Grisel, M. Blondel, P. Prettenhofer, R. Weiss, V. Dubourg, J. Vanderplas, A. Passos, D. Cournapeau, M. Brucher, M. Perrot, and E. Duchesnay, *Journal of Machine Learning Research* **12**, 2825 (2011).
- ²⁷ E. Metsanurk and M. Klintonberg, *Phys. Rev. B* **99**, 184304 (2019).
- ²⁸ G. Kresse and J. Furthmüller, *Phys. Rev. B* **54**, 11169 (1996).
- ²⁹ P. E. Blöchl, *Phys. Rev. B* **50**, 17953 (1994).
- ³⁰ G. Kresse and D. Joubert, *Phys. Rev. B* **59**, 1758 (1999).
- ³¹ J. P. Perdew, K. Burke, and M. Ernzerhof, *Phys. Rev. Lett.* **77**, 3865 (1996).
- ³² Y. Wang, J. J. Wang, W. Y. Wang, Z. G. Mei, S. L. Shang, L. Q. Chen, and Z. K. Liu, *Journal of Physics: Condensed Matter* **22**, 202201 (2010).
- ³³ F. Eriksson, E. Fransson, and P. Erhart, *Advanced Theory and Simulations* **2**, 1800184 (2019).
- ³⁴ C. Wang, M. Zinkevich, and F. Aldinger, *Journal of the American Ceramic Society* **89**, 3751 (2006).
- ³⁵ A. Kuwabara, T. Tohei, T. Yamamoto, and I. Tanaka, *Phys. Rev. B* **71**, 064301 (2005).
- ³⁶ Q.-J. Hong, S. V. Ushakov, D. Kapush, C. J. Benmore, R. J. K. Weber, A. van de Walle, and A. Navrotsky, *Scientific Reports* **8**, 14962 (2018).
- ³⁷ K. A. Irshad, V. Srihari, D. S. Kumar, K. Ananthasivan, and H. Jena, *Journal of the American Ceramic Society* **103**, 5374 (2020).